ENSEMBLE PREDICTION
AT THE EUROPEAN CENTRE FOR MEDIUM-RANGE WEATHER FORECASTS

Roberto Buizza

European Centre for Medium-Range Weather Forecasts

Summary. The current configuration of the European Centre for Medium-Range Weather Forecasts (ECMWF) Ensemble Prediction System (EPS) comprises 32 perturbed and one unperturbed non-linear integrations, at T63 spectral triangular truncation and with 19 vertical levels (32*T63L19). The perturbed initial conditions are generated using the most unstable directions growing over a 48-hour time period, computed at T42L19 resolution. The EPS performance during the first 18 months of daily operation is discussed. It shows that the probability of including the analysis within the EPS forecast range is still too low, due to a too small ensemble spread. It is argued that this is related to the T63L19 model not having a realistic activity, or to the ensemble size being too small. Two strategies to improve the EPS performance, one based on an ensemble system with higher resolution non-linear integrations (32*T106L19) and the other on a larger ensemble size (128*T63L19), are discussed. Preliminary results suggest that during some cases the increase of the model resolution could be necessary to improve the EPS performance, while in other cases the spanning of more unstable directions could be essential to increase the probability of having the analysis inside the EPS forecast range.

1. INTRODUCTION

Ensemble prediction can integrate a deterministic forecast with an estimate of the probability distribution function of atmospheric states, and thus has the capability of estimating the forecast skill of a deterministic forecast.

Since December 1992, both the U. S. National Meteorological Centre (NMC) and ECMWF have integrated their deterministic high-resolution prediction with medium-range ensemble prediction (*Tracton and Kalnay*, 1993; *Palmer et al*, 1993). The development follows the theoretical and experimental work of *Epstein* (1969), *Gleeson* (1970), *Fleming* (1971a-b) and *Leith* (1974).

Both Centres follow the same strategy of providing an ensemble of forecasts computed with the same

model, one started with unperturbed initial conditions referred to as the 'control' forecast, and an ensemble started with initial conditions defined by adding small perturbations to the control initial condition. Apart from differences in the ensemble size and the fact that at NMC a combination of lagged forecasts is used, the NMC and the ECMWF approaches to ensemble prediction differ substantially in the definition of the perturbations added to the control initial conditions to generate the initial conditions of the perturbed forecast. We refer the reader to *Toth and Kalnay* (1993) for the description of the 'breeding' method applied at NMC, and to *Buizza and Palmer* (1995) for a thorough discussion of the singular vector approach followed at ECMWF.

The first part of this paper briefly describes the ECMWF Ensemble Prediction System (the reader is referred to *Molteni et al*, 1996, for a more complete report). The successful implementation of the ECMWF Ensemble Prediction System (hereafter EPS) follows early experiments by *Hollingsworth* (1980), who demonstrated that a sparse random sampling of phase space does not produce a realistic distribution of forecast states, and ensemble forecasting experiments in which unstable singular vectors computed from a 3-level quasi-geostrophic model were used to generate the initial perturbation (*Mureau et al*, 1993, *Molteni and Palmer*, 1993).

In the second part of this paper the EPS performance during the first 18 months of daily operation are discussed. In particular, following *Buizza* (1996), attention is focused on three requirements: *i) the ensemble spread should be comparable to the skill of the control forecast, ii) small spread should indicate high probability of a skilful control forecast*, and *iii) the verifying analysis should be included within the range of ensemble forecasts*. The skill of the ensemble-mean is also discussed.

Finally, preliminary results of ongoing experimentation aimed to design a more skilful ensemble system will be presented.

The paper is organized as follows. After this Introduction, the ECMWF EPS is described in Section 2, the EPS performance is discussed in Section 3, preliminary results of future EPS upgrading are presented in Section 4, and some conclusions are drawn in Section 5.

2. THE ECMWF ENSEMBLE PREDICTION SYSTEM

The ECMWF EPS comprises, at the moment of writing, 32 perturbed and one unperturbed (control) non-linear integrations of a version of the ECMWF model (*Simmons et al*, 1989, and *Courtier et al*,

1991) with spectral triangular truncation T63 and 19 vertical levels (T63L19). The brief description of the EPS reported hereafter is integrated by the analysis of the ensemble forecast with a randomly chosen starting date, 95.11.05.

The initial conditions of the 32 perturbed members are created by adding and subtracting perturbations to the control initial conditions. The initial perturbations are defined using the singular vectors (*Buizza and Palmer*, 1995) of a linear approximation of the ECMWF model. The singular vectors identify the most unstable directions of the phase space of the system growing over a finite time interval named the optimisation time interval, where the growth of any perturbation is computed as the ratio between the perturbation total energy at optimisation and initial time (i.e. a total energy norm is used). An upper bound to the choice of the optimisation time interval is given by the time limit up to which the time evolution of small perturbations, with an initial amplitude comparable to an analysis error field, can be linearly approximated. *Buizza* (1995) estimated this time limit to be approximately 2 days. Concerning the choice of horizontal resolution, *Buizza et al* (1995) showed that singular vector with a T42 resolution are more capable to describe the growing part of forecast errors than T21 singular vectors.

At the moment of writing, the singular vectors are computed at T42L19 resolution with an optimisation time interval of 48 hours, following a time evolving trajectory computed applying the complete ECMWF physical package, but using only a linear surface drag and vertical diffusion scheme (*Buizza*, 1994) when computing linear forward and adjoint integrations (Table 1).

Figure 1 shows the singular values, i.e. the ratio between the singular vectors total energy norm at optimisation and initial time, for the 95.11.05 case (the singular vectors are ranked with respect to the singular values). For this case, 38 singular vectors have been computed after performing 70 integrations of the forward/adjoint models, using a Lanczos algorithm (*Strang*, 1986). The singular vectors have very localized structures, and grow in the regions of maximum instability of the atmosphere [*Buizza and Palmer* (1995) showed that there is a very strong relation between the singular vectors localization and a simple measure of both barotropic and baroclinic energy growth given by the growth rate of the most unstable Eady mode (*Hoskins and Valdes*, 1990)].

Figure 2 shows three singular vectors for the 95.11.05 case, at initial and optimisation time. The first singular vector is growing across the eastern border of the Asian continent, a region characterized by a very intense and rapid development (Fig. 3). By contrast, the third and the sixth singular vectors

are amplifying in relatively less unstable regions, as it is reflected by their smaller singular values. The different flow characteristics of the Asian, Pacific and European regions influence not only the singular values, but also the vertical structure of the singular vectors, especially at optimisation time. In fact, while the total energy of the first singular vector has a double maxima in the vertical, with a predominant low-level growth, the third and the sixth singular vectors have a more common vertical profile peaking at optimisation time around model level 9 (Fig. 4).

These three singular vectors are among the 16 selected from the 38 computed singular vectors. The selection criteria are such that the first 4 singular vectors are always chosen, and each subsequent singular vector (from the 5th onwards) is selected only if half of its total energy lies outside the regions where the singular vectors already selected are localized.

Once the 16 singular vectors have been selected, an orthogonal rotation in phase-space and a final re-scaling are performed to construct the ensemble perturbations. The purpose of the phase-space rotation is to generate perturbations which have the same globally-averaged energy as the singular vectors, but smaller local maxima and a more uniform spatial distribution. Moreover, the rotated singular vectors are characterized by similar amplification rates (at least up to 48 hours). The rotation is defined to minimize the local ratio between the perturbation amplitude and the amplitude of the analysis error estimate given by the ECMWF Optimum Interpolation procedure. At the moment of writing, the re-scaling allows perturbations to have local maxima up to $\alpha = \sqrt{1.5}$ larger than the local maxima of the analysis error estimate. The effect of the phase-space rotation and re-scaling procedures can be seen by comparing the singular vectors of Fig. 2 with three initial perturbations shown in Fig. 5.

The 16 perturbations are added and subtracted to the control initial conditions to define 32 perturbed initial conditions. Then, 32+1 (control) 10-day T63L19 non-linear integrations are performed. With the current ECMWF computer facilities (CRAY C90 with 16 processors), the elapsed time needed to compute 35-40 singular vectors amounts to approximately 0.8 hour, the elapsed time needed for generating the initial perturbations to 0.1 hour, and the elapsed time needed to perform the 33 non-linear integrations to approximately 1.8 hour. Thus, the total elapsed time is approximately 2.7 hours, which is about 1.3 times the elapsed time needed to performed the 10-day T213L31 ECMWF operational forecast.

A first way of verifying the EPS performance is to analyze the spread and the skill characteristics over different areas (see Fig. 6 for the 95.11.05 case over NH). The spread of a perturbed member is

defined by the anomaly correlation (acc) or root-mean-square (rms) distance between the perturbed ensemble member and the control, while the skill of a forecast is defined by the acc or the rms distance between the forecast and the analysis (see *Buizza*, 1996, for a mathematical definition).

Concerning EPS modifications, both model changes and revisions of the methodology used to generated the initial perturbations alter the EPS. The major model changes since EPS started (92.12.19) occurred on 93.08.04, when the new ECMWF surface and boundary layer scheme was introduced (*Viterbo and Beljaars*, 1995), and on 95.04.04, when the new ECMWF prognostic cloud scheme (*Tiedtke*, 1993, *Jacob*, 1994) and a new scheme for the representation of the sub-grid scale orography (*Lott and Miller*, 1995) were implemented. Table 2 lists the major changes of the configuration used to generate the perturbed initial conditions (see *Buizza*, 1996, for more details).

3. VALIDATION OF THE ECMWF EPS

3.1 Ensemble spread, and skill of the control forecast and of the ensemble-mean

Figure 7 shows the 5-day running mean of the skill of the control forecast, the skill of the ensemble-mean, and the average spread during a warm and a cold season (acc instead of rms values are shown since they are less seasonally dependent). The control acc skill is lower than the average spread, especially during the NH warm seasons. This is confirmed by the ratio between the rms error of the control and the average rms spread (Table 3). The enhancement of the difference during the NH warm seasons could be due to the EPS initial perturbations being computed with a dry linear forward and adjoint model, and to moist processes playing a more important role during the NH warm than cold seasons [*Errico and Ehrendorfer* (1995) showed that the inclusion of moist processes in the singular vector computation changes singular vector growth rates and structures.]

As shown in Table 3, the ratio between the control rms error and the rms spread is larger between day 5 and 7: this can be explained by the energetic characteristics of the T63L19 version of the ECMWF model, compared to the atmosphere or to the operational high resolution (T213L31) version of the ECMWF model. As *Simmons et al* (1995) pointed out, the level of transient activity in the forecast model should be similar to the transient activity in the analysis. *Tibaldi et al* (1990), comparing earlier versions of the ECMWF model at different resolutions, showed that at T63L19 resolution the model was not able to ensure the right level of change during the whole 10-day forecast period. Recent investigations confirm that this problem is still present in the current T63L19 version of the ECMWF model (*Anders Persson*, personal communication 1995). The lack of model activity could be cured,

at least in part, by using a higher resolution model version when performing the non-linear integrations. Note that, in fact, while the T106L19 model version used by *Tibaldi et al* (1990) was not performing significantly better than the T63L19 version, the current T106L19 model version is characterized by a more realistic model activity.

A complete picture of the average EPS performance over NH is given by Fig. 8. Generally speaking, the ensemble-mean is more skilful than the control forecast after forecast day 5, with differences in acc skill up to 0.10 for NH, and 0.14 for Europe, as highlighted in Table 4. Table 4 also summarizes the difference in acc skill of the best forecast with respect to the control forecast, at forecast day 5 and 7 over NH and Europe. The difference is skill between the best ensemble member and the control could be considered as an estimate of the best skill that could have been achieved by the EPS.

Both Fig. 8 and Table 3 confirm that the increase in the initial perturbation amplitude occurred on 94.08.23 reduced the difference between spread and control error, but despite the changes implemented on 95.03.14 (perturbations generated using T42 singular vectors but with smaller initial amplitude) the spread is still too small. When the 95.03.14 modifications were introduced, the perturbation initial amplitude was set to obtain slightly more spread than with the previous system. Since T42 singular vectors are more unstable than T21 singular vectors, this resulted in a net reduction of the perturbations initial amplitude. The lack of spread measured afterwards seems to be related to the subsequent change implemented on 95.04.04 (new model version). In fact, the model version introduced on 95.04.04 seems to be less active and thus less able to sustain the perturbation growth (*A. Simmons*, personal communication, 1995; this has been confirmed by comparison of seasonal integrations of the new and the old model versions, *Č. Brancović*, personal communication, 1995, and by results obtained by *R. Gelaro*, who found a reduction in the model sensitivity fields between the new and the old model versions, personal communication 1995).

3.2 Percentage of skilful members

Figure 9 shows, for each season, percentages of EPS members with skill higher than defined thresholds, computed from probability distribution functions of ensemble skill (*Buizza*, 1996). Considering for example forecast day 7, 20% (30%) of the ensemble members have always acc skill higher than 0.60 over NH (Europe).

3.3 Correspondence between small spread and high skill

Tables 5a-d list the contingency tables and the correlation coefficients relative to scatter diagrams of

ensemble spread versus control skill at forecast day 5 (not shown) and 7 (Figs. 10-11) for NH and Europe. Slightly better correlations characterize forecast day 5 respect to day 7, especially over Europe (Tables 5b and 5d). Similarly, considering requirement *ii)* defined in the Introduction (small spread should indicate high probability of a skilful control forecast), a better agreement is achieved at forecast day 5 than 7.

3.4 Percentage of analysis values lying outside the EPS forecast range

Table 6 lists the percentage of analysis values lying outside the EPS forecast range for NH and Europe at forecast day 5 and 7. The seasonal variability of the percentages reflects the ratio between control error and ensemble spread, with seasons with larger percentages corresponding to seasons with higher ratios (compare Tables 3 and 6). Values are still quite high, especially at forecast day 5 over Europe. This could be seen as an indication that 32 members is a too small ensemble size.

4. FUTURE DEVELOPMENTS

As mentioned in Section 3.1, the EPS should benefit from an increase in the model resolution. Moreover, less inconsistency between the operational deterministic T213L31 and the EPS resolutions should improve the usefulness of the integrated **T213L31+EPS** Meteorological Operational System. However, a model resolution increase could not be sufficient, since as pointed out in Section 3.4 the current ensemble size seems to be too small. The ensemble size can be increased in different ways, e.g. by adding a set of perturbations pointing in the same direction (of the phase space of the system) as the one currently used but with different amplitude, or by perturbing along more directions. This latter is the strategy we are investigating at present, with extra directions defined by considering more than the currently used 16 singular vectors. Preliminary results of ensembles run with either more members or higher resolutions for two case studies are discussed hereafter (Table 7).

Figures 12 and 13 show the spread and the skill of ensembles run in configurations 32*T63L19, 128*T63L19 and 32*T106L19 for two cases, 94.12.12 and 95.01.12, over Europe (these are two among 14 winter cases selected to test new EPS configurations). Considering NH (not shown), there is an indication that the initial perturbations grow faster when non-linearly integrated with a higher resolution model, especially after forecast day 5. As mentioned in Section 3.1, this can be explained, at least partly, by the fact that the T106L19 model is characterized by a more realistic activity. By contrast, the spread of the 128*T63L19 is comparable to the spread of the 32*T63L19 configuration. In fact, the larger rms amplitude of the 128*T63L19 initial perturbations, due to the combination of

64 instead of 16 singular vectors, is compensated during the time integration by the fact that the 64 initial perturbations of configuration 128*T63L19 are characterized, on average, by smaller amplification rates than the 16 perturbations of configuration 32*T63L19. Indeed, they are generated considering not only the first 16 singular vectors but also singular vectors with decreasing order characterized, by definition, by smaller amplification rates (see, eg, Fig. 1).

The impact on the EPS skill of the configuration changes differs substantially during two cases. In fact, while a higher model resolution enhances the number of skilful medium-range forecasts for the 94.12.12 case (Fig. 12), the increase in model resolution does not produce any significant improvement in the EPS skill for the 95.01.12 case (Fig. 13).

Considering in more detail the 94.12.12 case, the resolution increase improves dramatically the skill of the best ensemble member (Fig. 14). Over Europe, for example, at forecast day 7, improvements in the acc skill of the ensemble-mean and of the best ensemble member of 0.16 and 0.37, respectively, can be detected. This is due to a better prediction of the high pressure ridge south-east of the cut-off low positioned over the Norwegian Sea (Fig. 14), and to a general decrease of the forecast error in the analyzed region (Fig. 15). The divergence of the best ensemble member from the control responsible for the skill improvement over Europe at forecast day 7 is mainly due to an initial perturbation over Alaska and Canada (Fig. 16). Note that initially, in terms of 500 hPa geopotential height, the added perturbation is locally smaller than 2.5m.

Consistently with the skill increase, the percentage of analysis values lying outside the forecast range reaches minimum values for, respectively, configurations 32*T106L19 and 128*T63L19 during the 94.12.12 and 95.01.12 cases (Table 8).

It is worth mentioning that during the ongoing experimentation the possibility of increasing the number of vertical levels will also be considered. Although it is too early to draw any conclusion, the outcome of the reported preliminary results indicates that a new EPS configuration with more ensemble members and higher resolution non-linear integrations (e.g. 50*T106L31, computer resources permitting, see Table 7) should be desirable.

5. CONCLUSIONS

Ensemble prediction through multiple integrations of a deterministic model estimates the probability distribution of atmospheric states. In the first part of this paper the ECMWF EPS, based on one unperturbed and 32 perturbed T63L19 integrations, has been briefly described. In particular, the main

steps of the construction of the perturbed initial conditions have been illustrated throughout of the analysis of one case study.

In the second part of this paper the performance of the ECMWF EPS has been discussed. Results show that the ensemble spread is still too small, especially in the second half of the 10-day forecast period. The comparison between ensemble spread and control forecast skill have shown that their correlation is rather small in absolute terms. *Buizza* (1996), argued that a more correct analysis should be based on the comparison between real with potential forecast skill, the latter estimated by evaluating the ensemble performance with the verifying analysis defined by a randomly chosen ensemble member. If his approach is followed, although correlation coefficients of the EPS verified using the analysis are smaller than their potential counterparts, the difference between real and potential values are rather small. The ensemble-mean have been shown to be more skilful than the control after forecast day 5, with differences up to 0.10 (0.14) at forecast day 10 for NH (Europe). Consistently with too small ensemble spread, the percentage of analysis values lying outside the EPS forecast range is still quite large, especially at forecast day 5. This could indicate that the sub-space of the phase space of the system spanned by the ensemble perturbations is too small.

Finally, preliminary results of a comparison of the operational (32*T63L19) and two new ensemble configurations with either a higher resolution model (32*T106L19) or a larger ensemble size (128*T63L19) have been reported. The analysis of two case studies suggests that while some cases would benefit more from an increased model resolution, others would need more ensemble members to increase the probability of the analysis lying inside the EPS forecast range. Future implementation of an ensemble system with more members and higher resolution non-linear integration should improve the usefulness of the integrated **T213L31+EPS** Meteorological Operational System.

ACKNOWLEDGEMENTS

The author would like to thank Horst Böttger for useful comments given to a first version of this manuscript.

REFERENCES

Buizza, R, 1994. Sensitivity of optimal unstable structures. *Q. J. R. Meteorol. Soc.*, **120**, 429-451.

Buizza, R, 1995. Optimal perturbation time evolution and sensitivity of ensemble prediction to perturbation amplitude. *Q. J. R. Meteorol. Soc.*, **121**, 1705-1738.

Buizza, R, 1996. Potential forecast skill of ensemble prediction, and spread and skill distributions of the ECMWF Ensemble Prediction System. Proceedings of the ECMWF Seminar on *Predictability*, 4-8 September 1995, ECMWF, Shinfield Park, Reading RG2-9AX, UK. Also *M. Wea. Rev.*, submitted.

Buizza, R, and T N Palmer, 1995. The singular vector structure of the atmospheric general circulation. *J. Atmos. Sci.*, **52**, 9, 1434-1456.

Buizza, R, Gelaro, R, Molteni, F, and T N Palmer, 1995. Predictability studies with high resolution singular vectors. ECMWF Research Department Technical Memorandum n, 219, ECMWF, Shinfield Park, Reading RG2 9AX, U.K.. Also *Q. J. R. Meteorol. Soc.*, submitted.

Courtier, P, C Freyder, J F Geleyn, F Rabier and M Rochas, 1991. The Arpege project at Météo France. Pp. 192-231 in Proceedings of the ECMWF seminar on *Numerical methods in atmospheric models*, ECMWF, Shinfield Park, Reading RG2-9AX, 9-13 September 1991, Vol. 2.

Epstein, E S, 1969. Stochastic dynamic predictions. *Tellus*, **21**, 739-759.

Errico, E R, and M Ehrendorfer, 1995. Moist singular vectors in a primitive-equation regional model. American Meteorological prep-prints of the *Tenth conference on atmospheric and oceanic waves and stability*, June 5-9, 1995, Big Sky, Montana, 272 pp.

Fleming, R J, 1971a. On stochastic dynamic prediction. I: the energetics of uncertainty and the question of closure. *Mon. Wea. Rev.*, **99**, 851-872.

Fleming, R J, 1971b. On Stochastic dynamic prediction. II: predictability and utility. *Mon. Wea. Rev.*, **99**, 927-938.

Gleeson, T A, 1970. Statistical-dynamical predictions. *J. Appl. Meteorol.*, **9**, 333-344.

Hollingsworth, A, 1980. An experiment in Monte Carlo forecasting procedure. ECMWF workshop on *Stochastic dynamic prediction*, ECMWF, Shinfield Park, Reading RG2-9AX, UK. 99 pp.

Hoskins, B J, and P J Valdes, 1990. On the existence of storm tracks. *J. Atmos. Sci.*, **47**, 1854-1864.

Jacob, C, 1994. The impact of the new cloud scheme on ECMWF's Integrated Forecasting System (IFS). Proceedings of the ECMWF/GEWEX workshop on *Modelling, validation and assimilation of clouds*, ECMWF, Shinfield Park, Reading RG2-9AX, November 1994.

Leith, C E, 1974. Theoretical skill of Monte Carlo forecasts. *Mon. Wea. Rev.*, **102**, 409-418.

Lott, F, and M Miller, 1995. A new sub-grid scale orographic drag parametrization: its formulation and testing. ECMWF Research Department Technical Memorandum n. 218, ECMWF, Shinfield Park, Reading RG2-9AX. Also *Q. J. R. Meteorol. Soc.*, submitted.

Molteni, F, and T N Palmer, 1993. Predictability and finite-time instability of the northern winter circulation. *Q. J. R. Meteorol. Soc.*, **119**, 1088-1097.

Molteni, F, R Buizza, T N Palmer and T Petroliagis, 1996. The ECMWF ensemble prediction system: methodology and validation. *Q. J. R. Meteorol. Soc.*, **122**, 73-119.

Mureau, R, F Molteni and T N Palmer, 1993. Ensemble prediction using dynamically-conditioned perturbations. *Q. J. R. Meteorol. Soc.*, **119**, 269-298.

Palmer, T N, F Molteni, R Mureau, R Buizza, P Chapelet and J Tribbia, 1993. Ensemble prediction. ECMWF Seminar Proceedings on *Validation of models over Europe: Vol. 1*, ECMWF, Shinfield Park, Reading RG2 9AX, UK, 285 pp.

Simmons, A J, D M Burridge, M Jarraud, C Girard and W Wergen, 1989. The ECMWF medium-range prediction models development of the numerical formulations and the impact of increased resolution. *Meteorol. Atmos. Phys.*, **40**, 28-60.

Simmons, A J, R Mureau and T Petroliagis, 1995. Error growth and predictability estimates for the ECMWF forecasting system. ECMWF Research Department Technical Memorandum n. 201, ECMWF, Shinfield Park, Reading RG2-9AX. Also *Q. J. R. Meteorol. Soc.*, submitted.

Strang, G, 1986. *Introduction to applied mathematics*. Wellesley-Cambridge Press, 758 pp.

Tibaldi, S, T N Palmer, Č Brancović, and U Cubasch, 1990. Extended-range predictions with ECMWF models: influence of horizontal resolution on systematic error and forecast skill. *Q. J. R. Meteorol. Soc.*, **116**, 835-866.

Tiedtke, M, 1993. Representation of clouds in large-scale models. *Mon. Wea. Rev.*, **121**, 11, 3040-3060.

Toth, Z, and E Kalnay, 1993. Ensemble forecasting at NMC: the generation of perturbations. *Bull. Am. Met. Soc.*, **74**, 2317-2330.

Tracton, M S and E Kalnay, 1993. Operational ensemble prediction at the National Meteorological Center: practical aspects. *Weather and Forecasting*, **8**, 379-398.

Viterbo, P, and A C M Beljaars, 1995. An Improved land surface parametrization scheme in the ECMWF model and its validation. *J. Clim.*, **8**, 2716-2748.

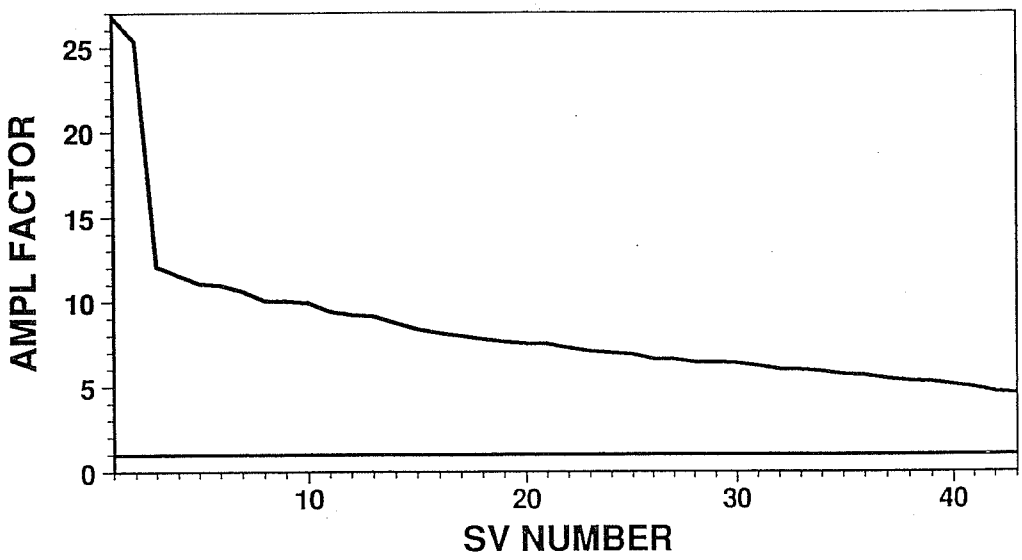

Fig 1 Singular values for 95.11.05 (the singular vectors are ranked with respect to their amplification rate).

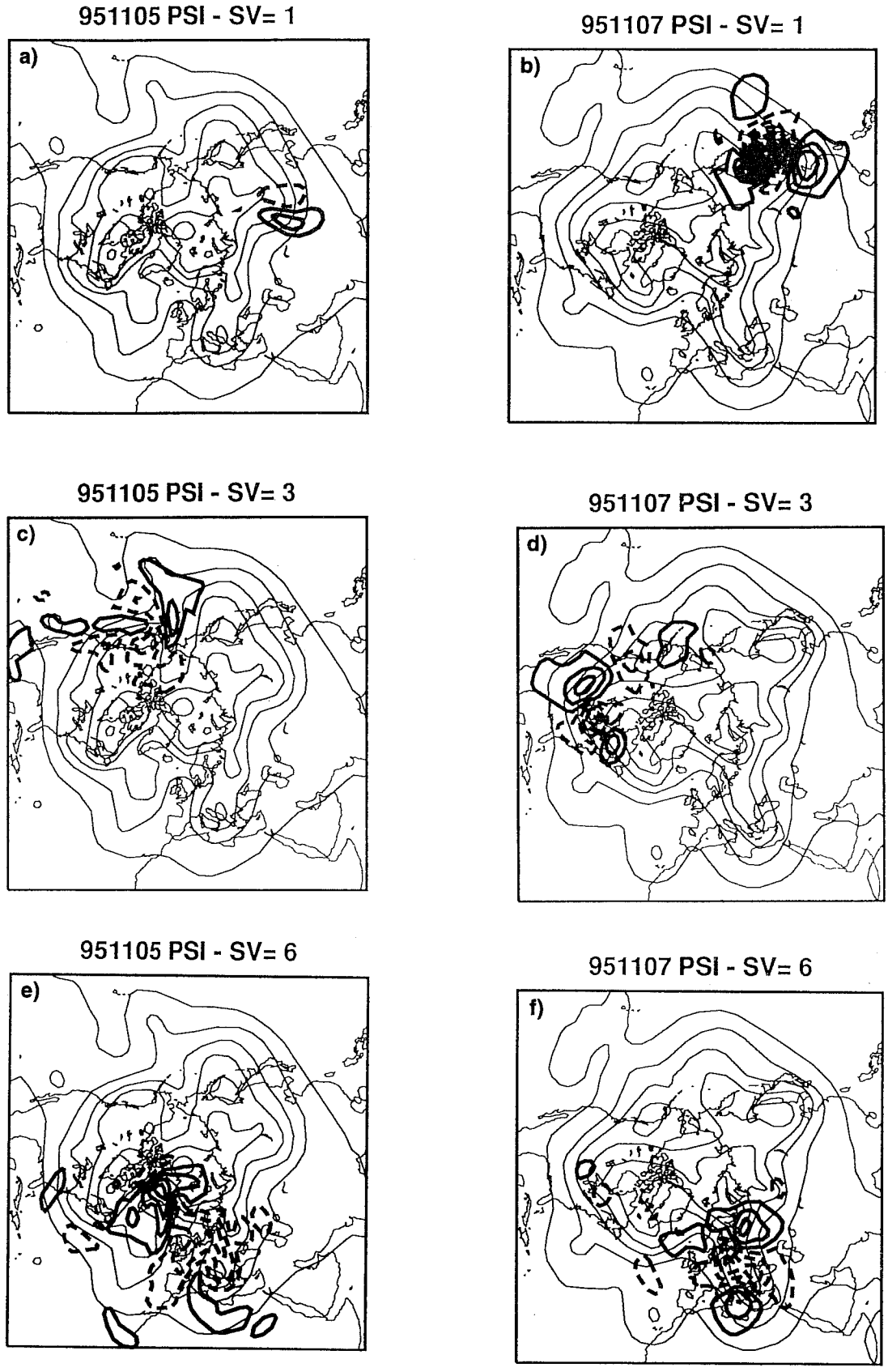

Fig 2 Singular vectors number 1 (top panels), 3 (middle panels) and 6 (bottom panels) at initial (left panels) and optimisation time (right panels). Each panel shows the singular vector streamfunction at model level 11 (approximately 500 hPa), superimposed to the trajectory 500 hPa geopotential height field. Streamfunction contour interval for left panels and 20 times larger for right panels; geopotential height contour interval .

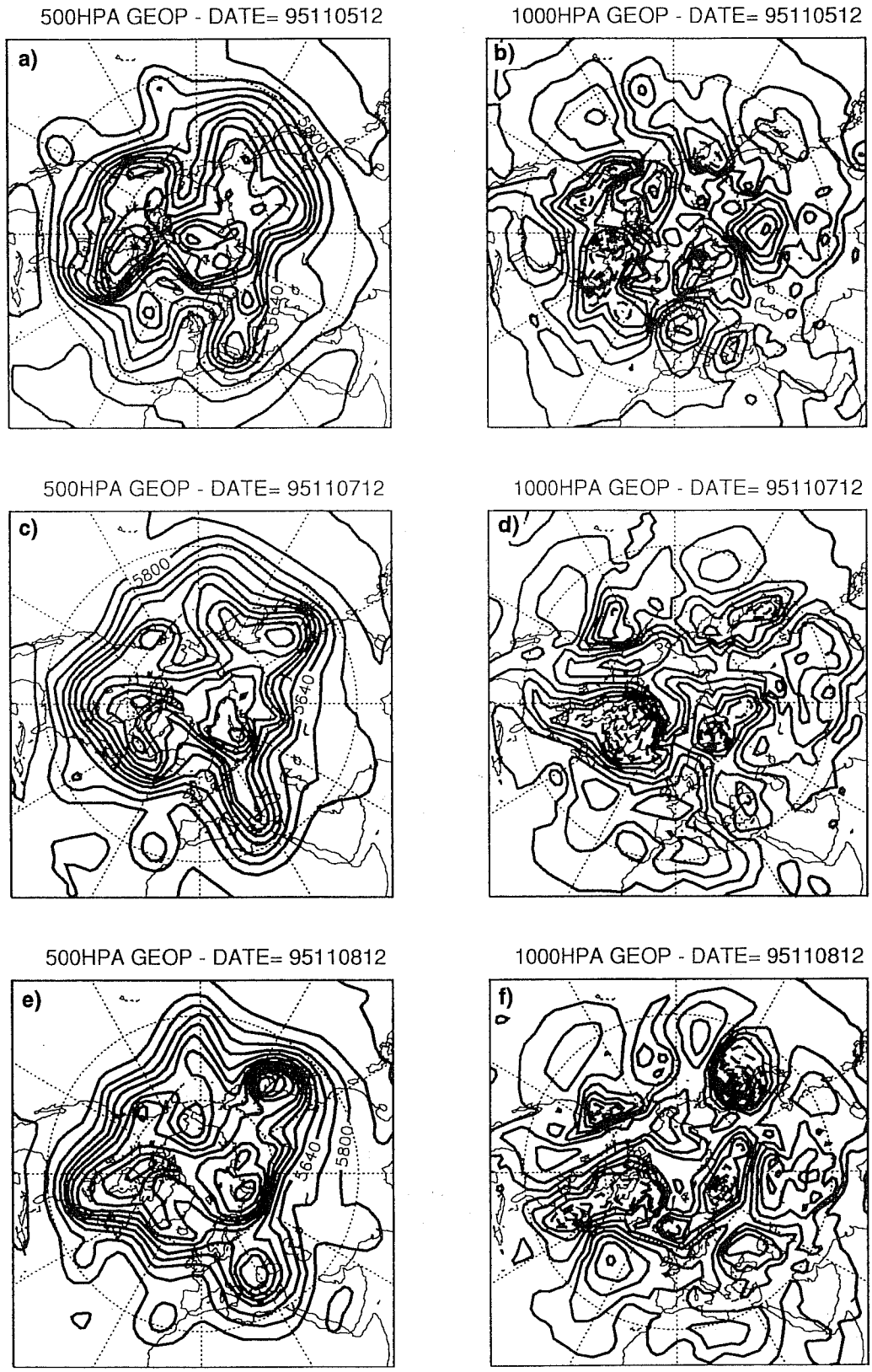

Fig 3 500 hPa (left panels) and 1000 hPa (right panels) geopotential height (left panels) trajectory for the 5th, the 7th and the 8th of November 1995. Contour intervals for left panels, and for right panels.

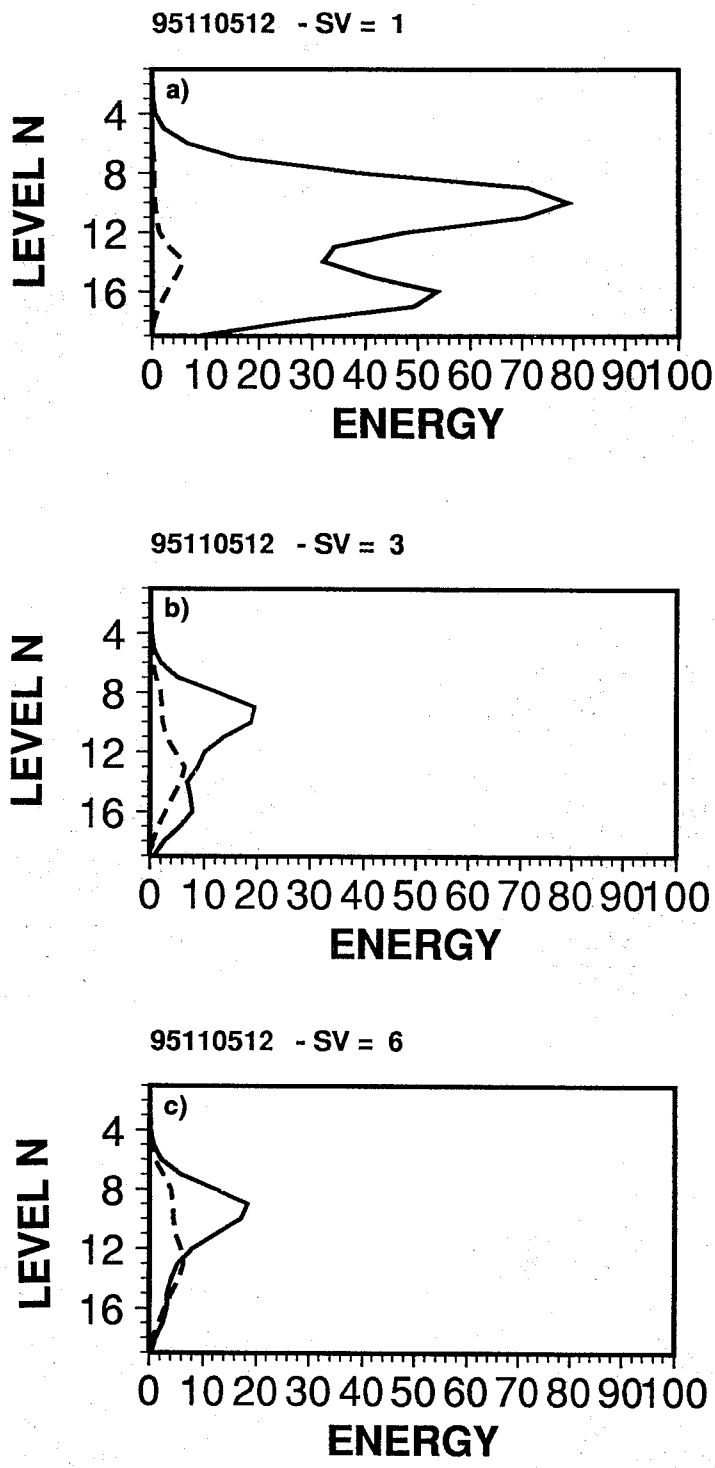

Fig 4 Total energy () vertical profile of the (a) 1st, (b) 3rd and (c) 6th singular vector of 95.11.05, at initial (dash line, values multiplied by 100) and optimisation (solid line) time. (Note that singular vectors are normalized to have unit initial total energy norm.)

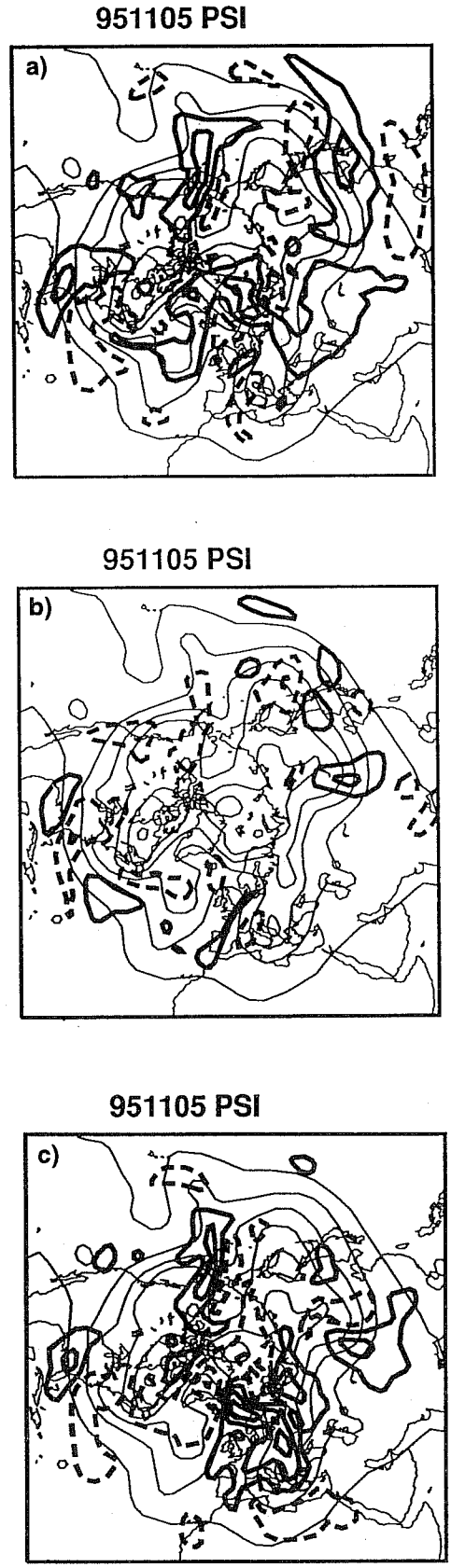

Fig 5 As Fig. 2 but for three perturbations (streamfunction) generated applying the phase-space rotation and re-scaling procedure to the selected singular vectors, superimposed to the trajectory 500 hPa geopotential height field. Contour interval for streamfunction, and 80 m for geopotential height.

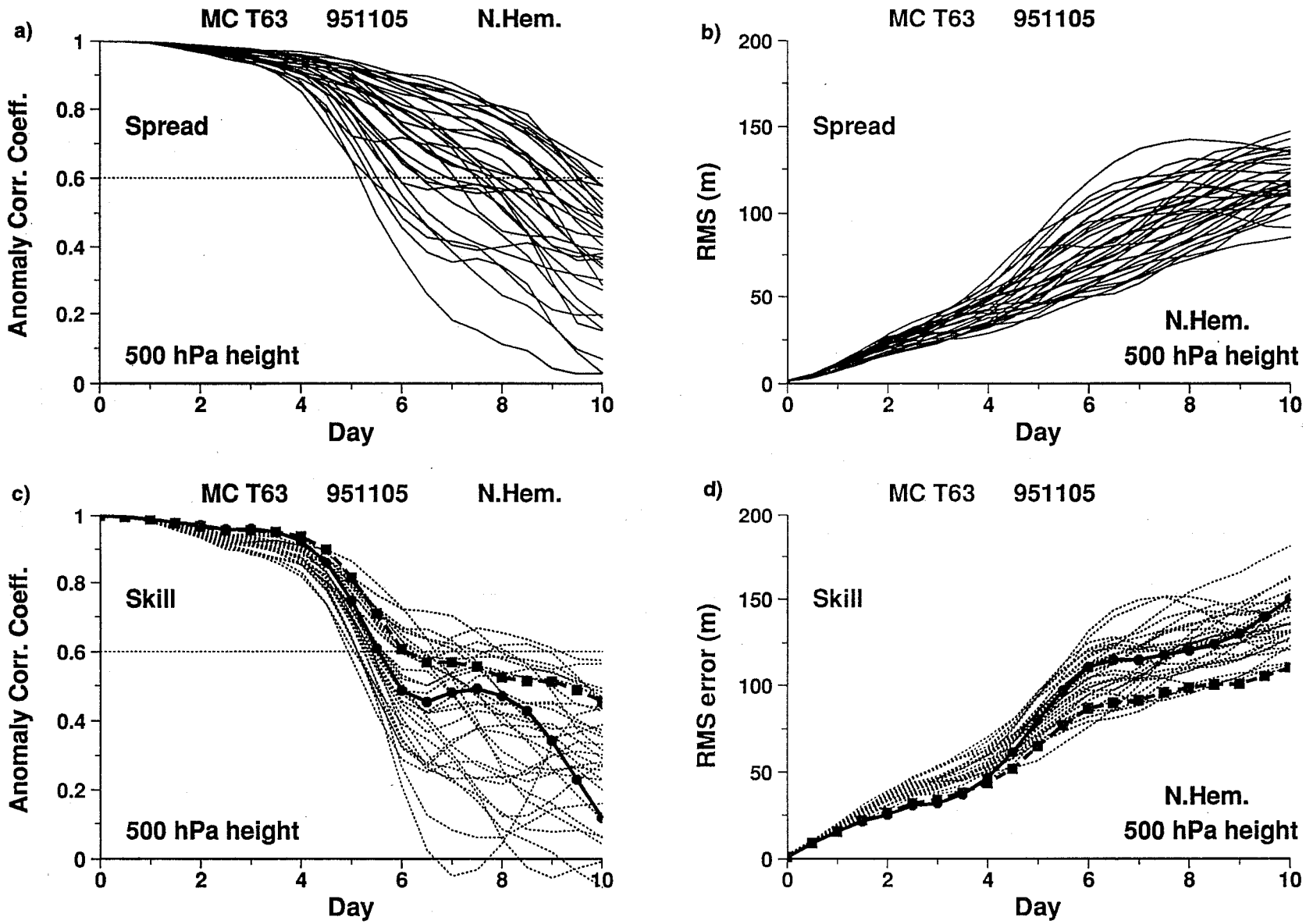

Fig 6 Spread (left panels) and skill (right panels), of the EPS run with starting date 95.11.05, computed for the 500 hPa geopotential height over NH. Top panels refers to acc and bottom panels to rms values.

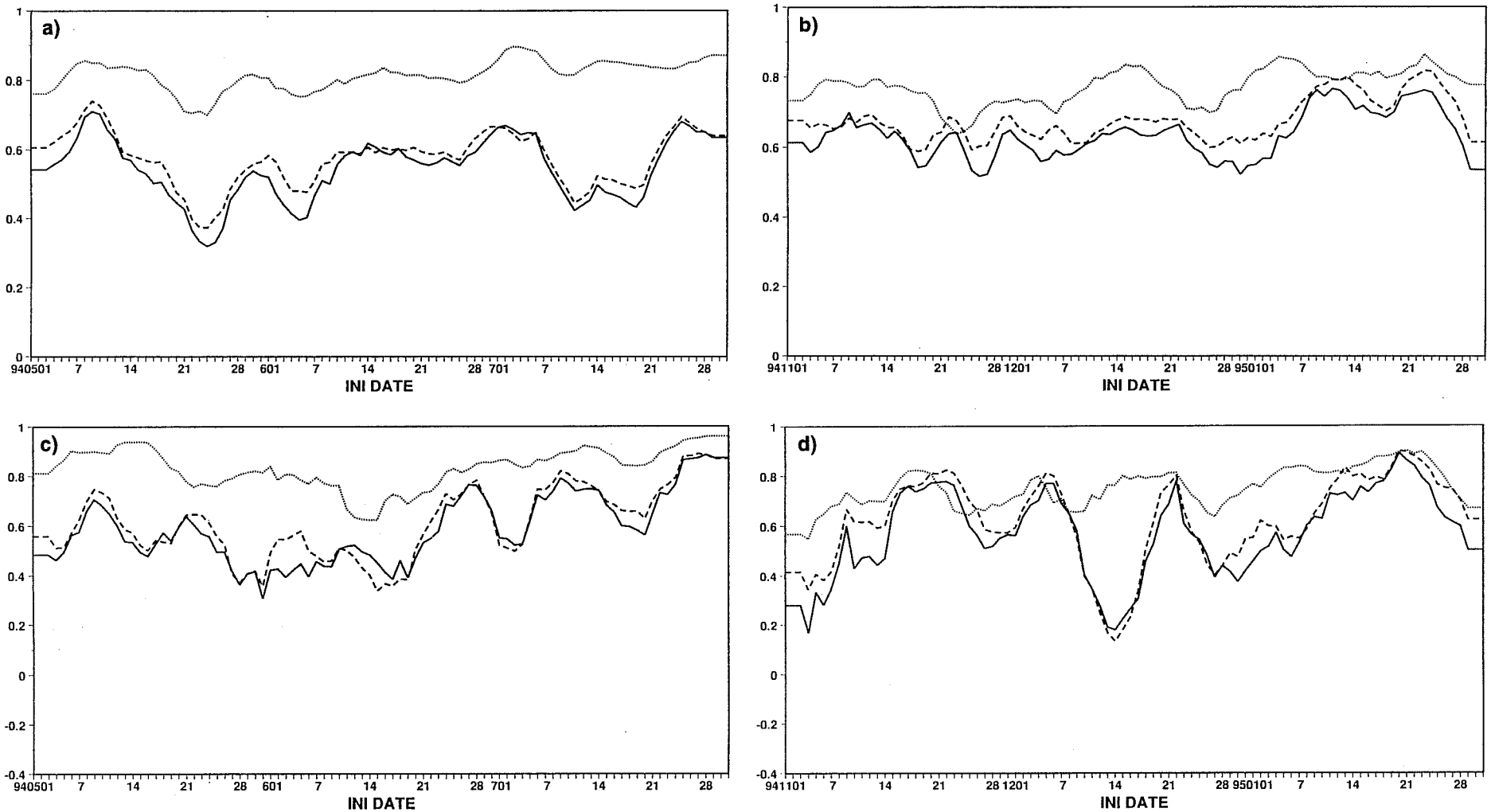

Fig 7 Control skill (solid), ensemble-mean skill (dash) and average spread (dot) for: (a) 94.05.01-94.07.31, NH; (b) 94.11.01-95.01.31, NH; (c) as a) but for Europe; (d) as b) but for Europe. Values refer to 500 hPa geopotential height.

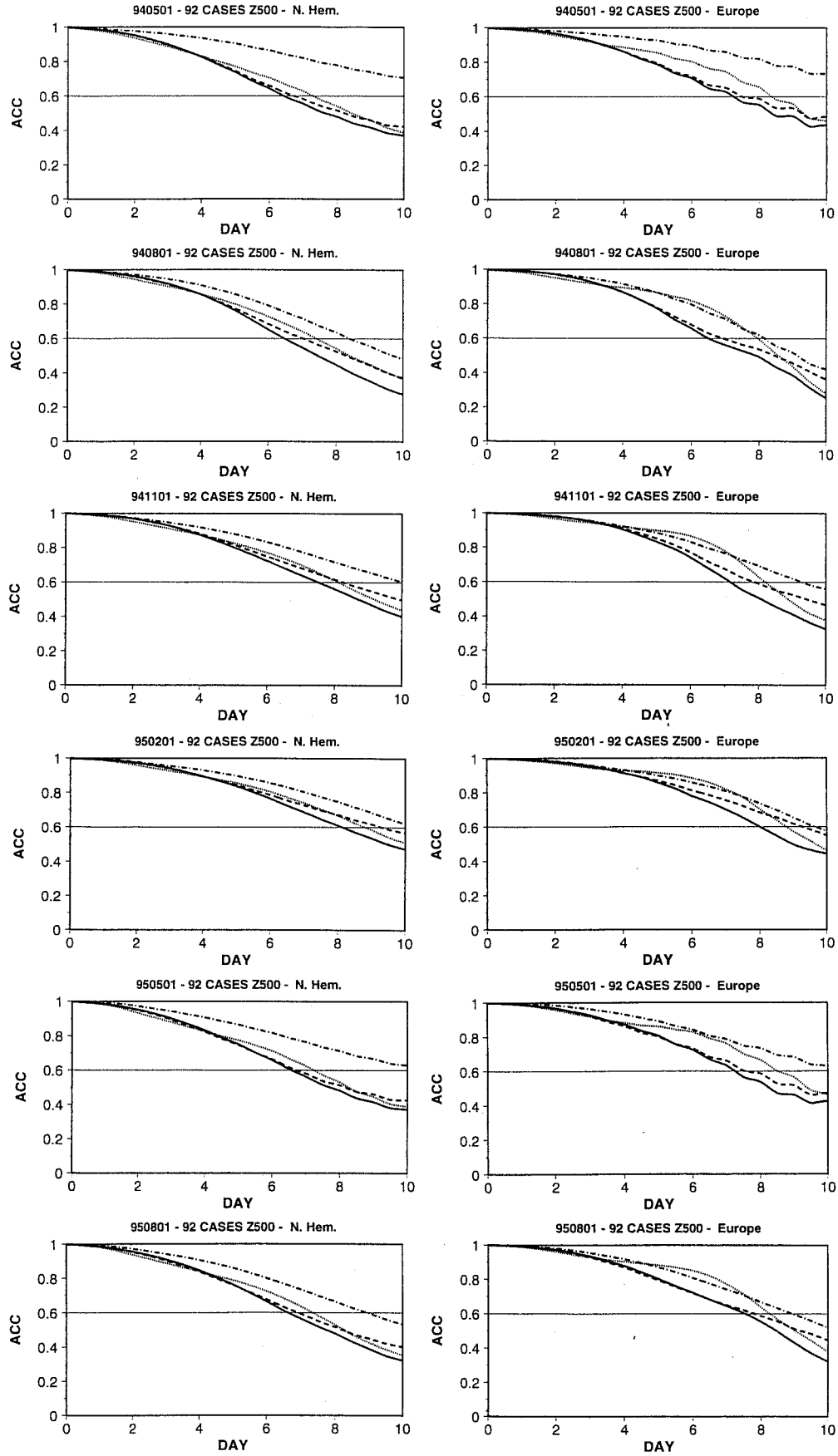

Fig 8 Control skill (solid), ensemble-mean skill (dash), best ensemble member skill (defined as the ensemble member with the highest skill between day 4 and 7, dot), and average spread (chain-dash) for the six 92-day seasons, computed for the 500 hPa geopotential height over NH (left panels) and Europe (right panels).

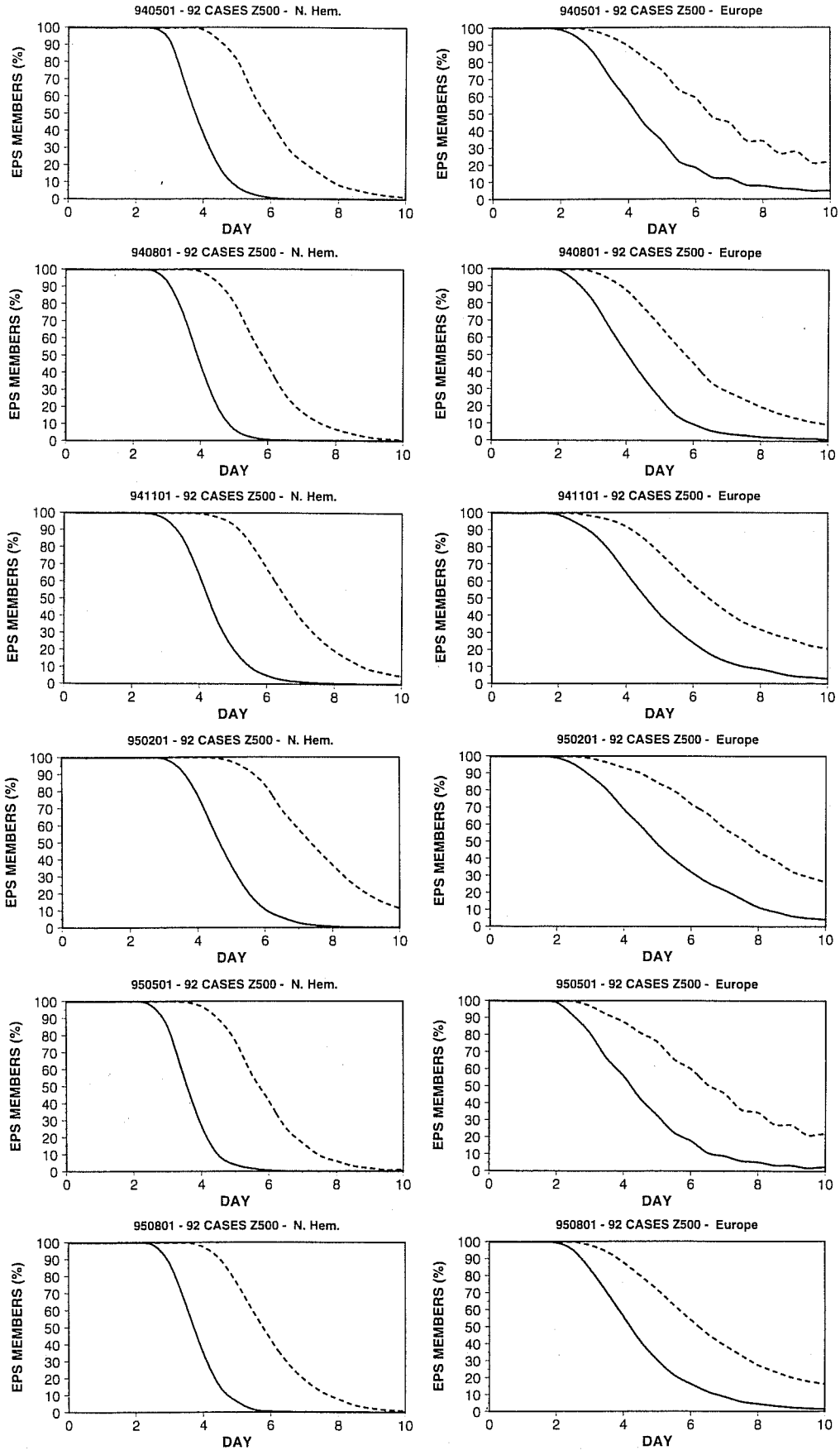

Fig 9 Percentage of EPS members with acc skill higher than 0.8 (solid) and 0.6 (dash), for the 92-day seasons, computed for the 500 hPa geopotential height over NH (left panels) and Europe (right panels).

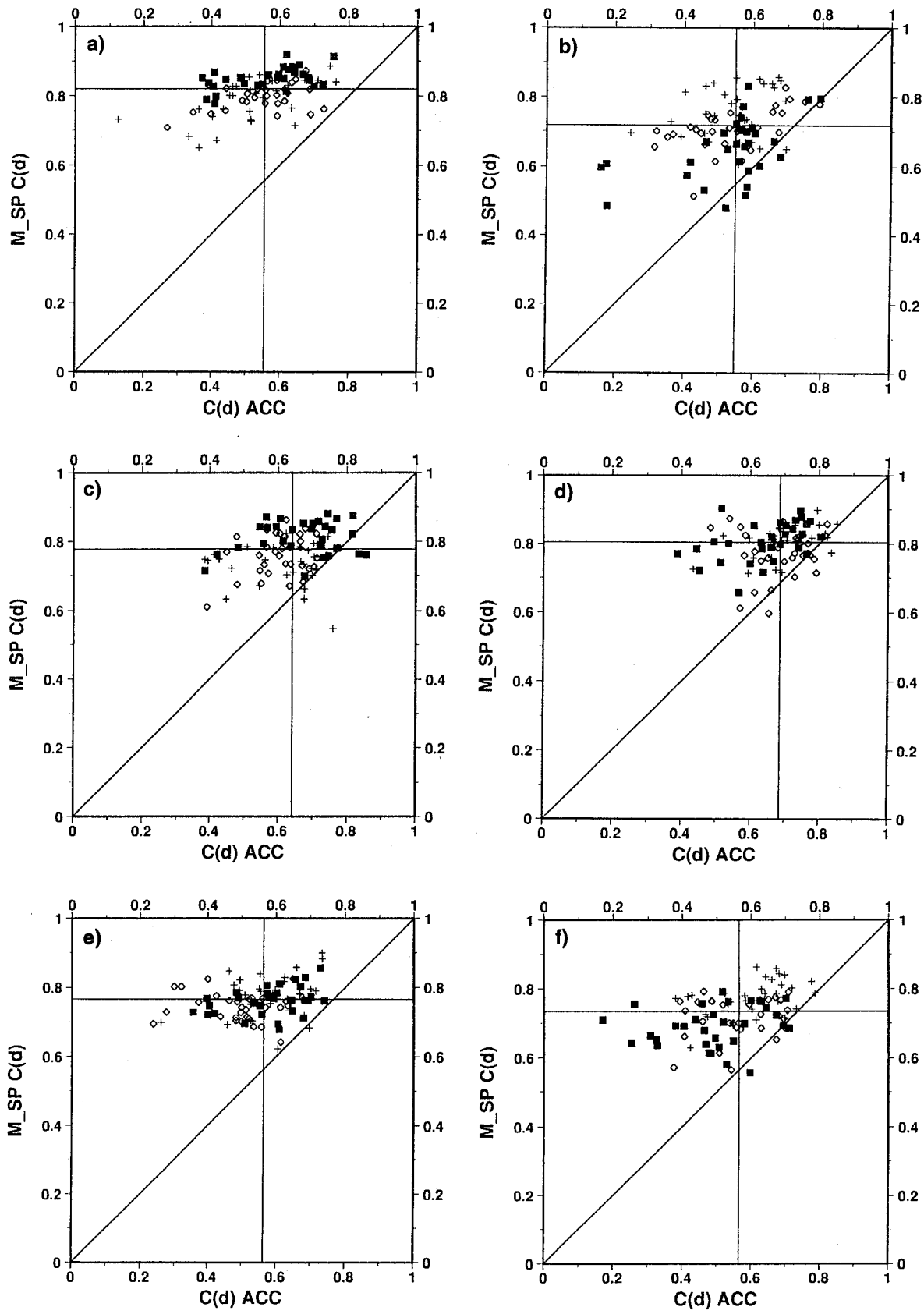

Fig 10 Scatter diagrams of EPS spread versus control skill for the six 92-day seasons starting a) 94.05.01, b) 94.08.01, c) 94.11.01, d) 95.02.01, e) 95.05.01 and f) 95.08.01. Values refer to the 500 hPa geopotential height over NH, at forecast day 7. For each season, plus-diamond-square markers in the scatter diagram identify cases of the first-second-third month of the analyzed season.

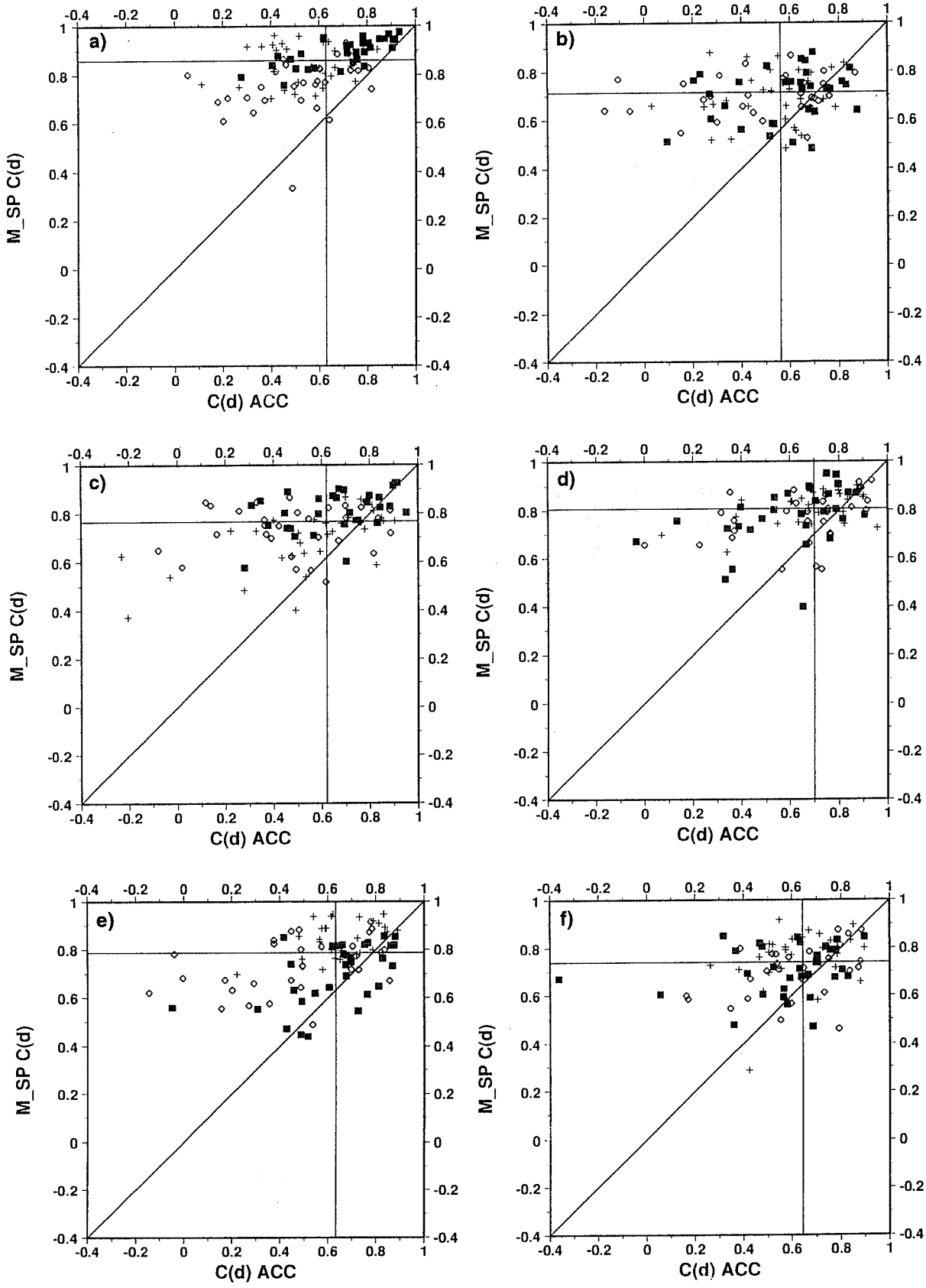

Fig 11 As Fig. 10 but for Europe.

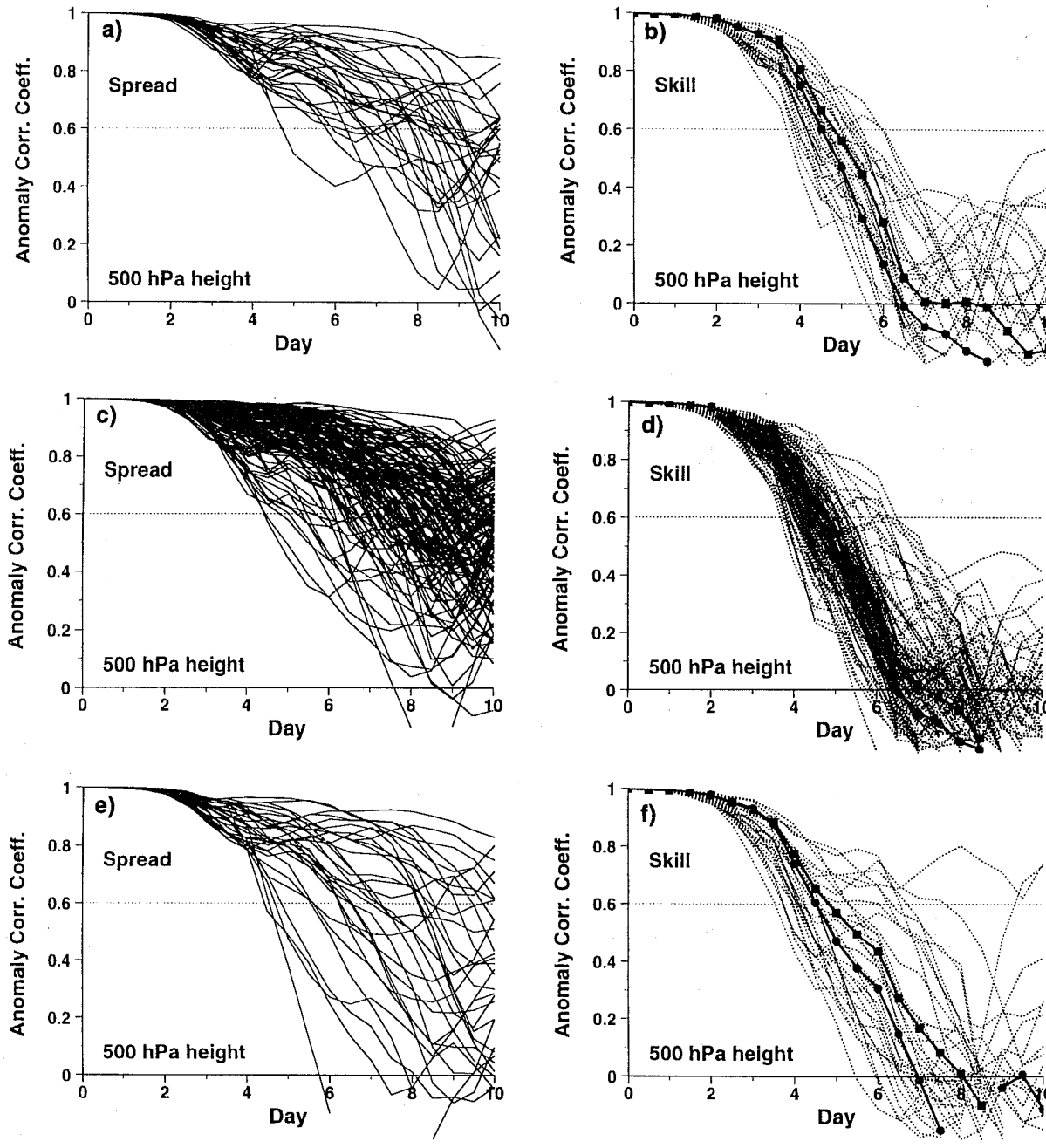

Fig 12 Spread (left panels) and skill (right panels) of ensembles run in configurations 32*T63L19 (top), 128*T63L19 (middle) and 32*T106L19 (bottom), for the 94.12.12 case. The acc values have been computed using the 500 hPa geopotential height field over Europe.

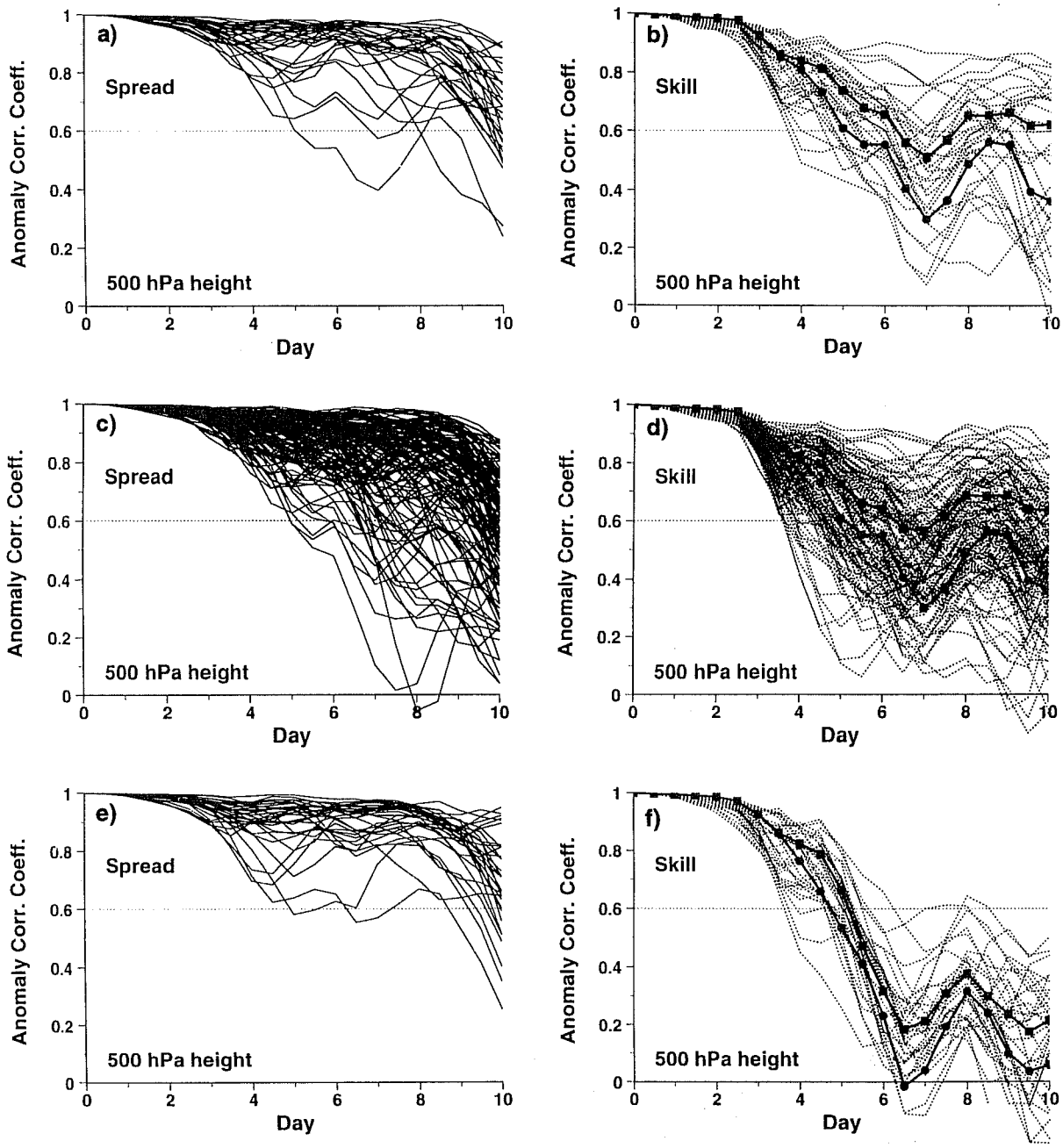

Fig 13 As Fig. 12 but for the 95.01.12 case.

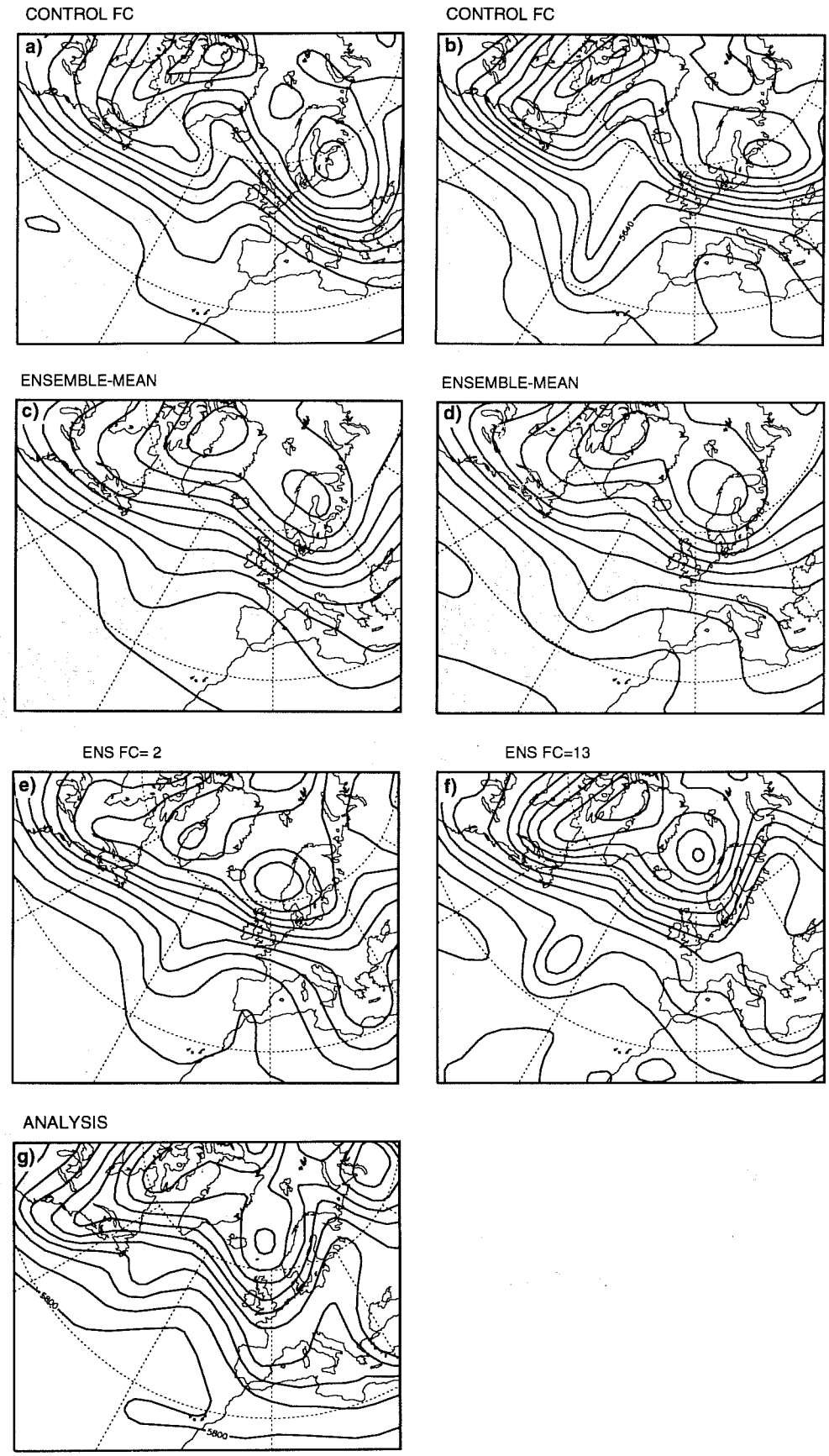

Fig 14 94.12.12 case: 500 hPa geopotential height fields for: (a): control forecast at day 7 from configuration 32*T63L19; (b): as (a) but for configuration 32*T106L19; (c): ensemble-mean forecast from configuration 32*T63L19; (d): as (c) but for configuration 32*T106L19; (e): best forecast from configuration 32*T63L19; (f): as (e) but for configuration 32*T106L19; (g): analysis for 94.12.19, i.e. corresponding to day 7 forecasts started on 94.12.12. Contour interval 80 m.

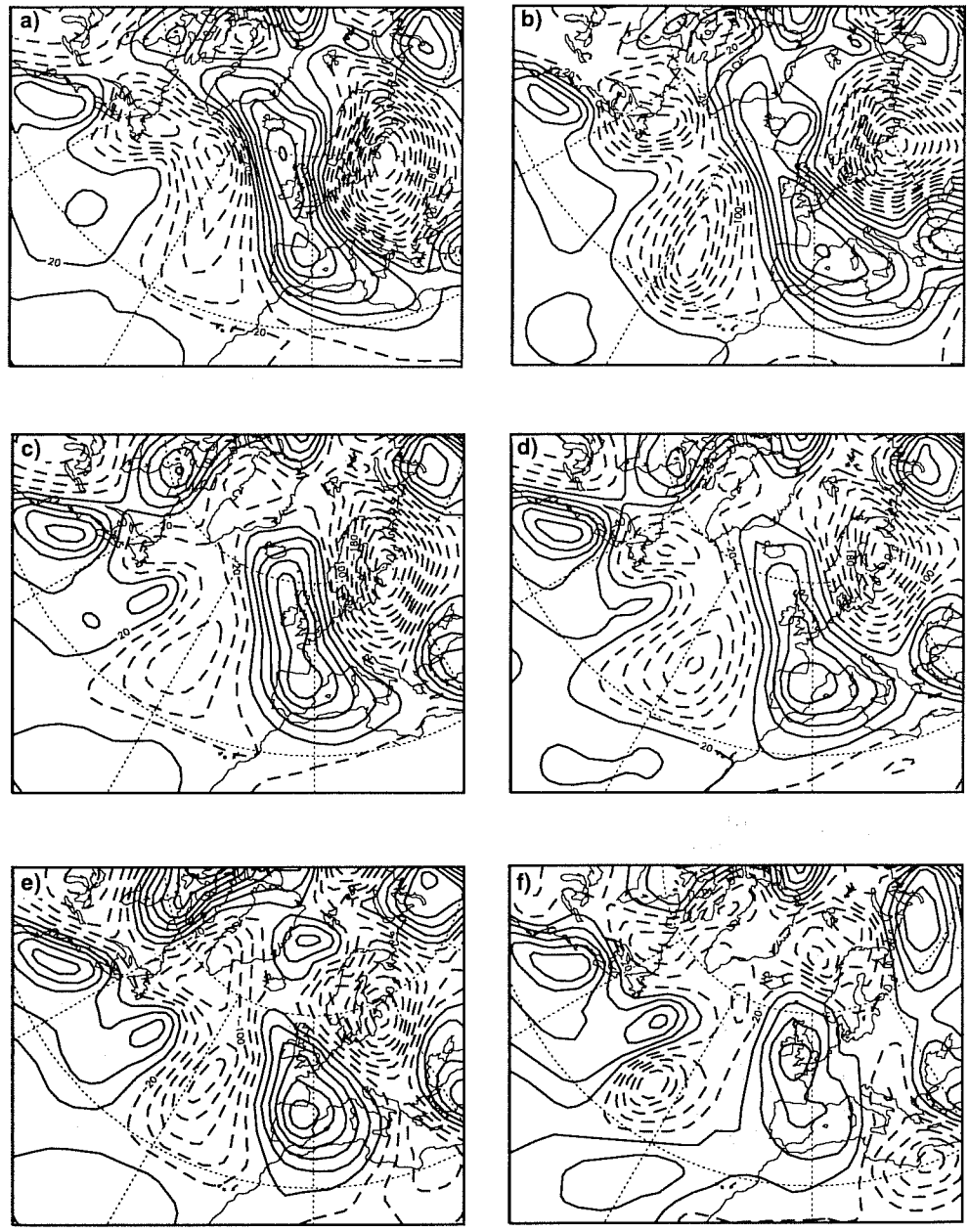

Fig 15 94.12.12 case: error of the 500 hPa geopotential height forecasts for: (a): control forecast at day 7 from configuration 32*T63L19; (b): as (a) but for configuration 32*T106L19; (c): ensemble-mean forecast from configuration 32*T63L19; (d): as (c) but for configuration 32*T106L19; (e): best forecast from configuration 32*T63L19; (f): as (e) but for configuration 32*T106L19. Contour interval 40 m.

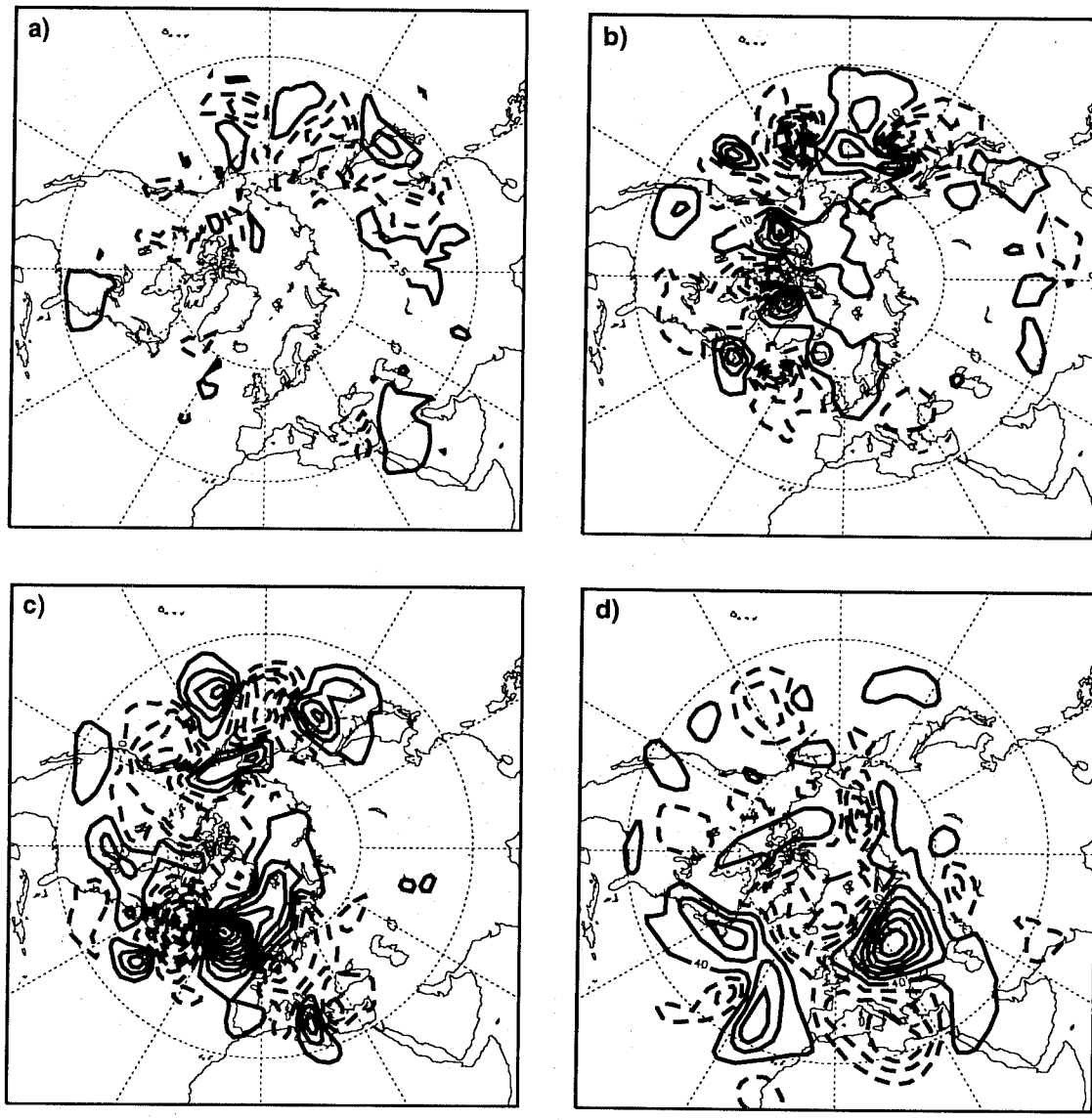

Fig 16 94.12.12: difference field between the best and the control forecast, in terms of 500 geopotential height field, at (a) initial time, and at forecast day (b) 2, (c) 4 and (d) 7. Contour interval (a) 5m starting form 2.5m, (b) 20m starting from 10m, (c) 40m starting from 20m, and (d) 80m starting from 40m, with dashed lines for negative values.

Horizontal resolution:	T42 spectral triangular truncation.
Vertical resolution:	19 vertical levels.
Optimisation time interval:	48 hours.
Diabatic schemes in direct:	full physics.
Diabatic schemes in forward/adjoint:	linear physics and horizontal diffusion.
Local Projection Operator:	$\phi \geq 30°N$.

Table 1 Characteristics of the singular vector computation used at the time of writing.

92.12.19	EPS starting date. The EPS is run weekly on Saturdays, Sundays and Mondays, with T21L19 global singular vectors, maximized over a 36 hour time interval, with initial amplitude scaled with $\alpha = \sqrt{2}$.
93.02.20	The singular vectors are maximized only over the NH extra-tropics ($\phi \geq 30°N$).
94.05.01	EPS starts being run daily.
94.08.23	The singular vectors optimisation time interval is increased from 36 to 48 hours, and the perturbation initial amplitude is increased, $\alpha = 2$.
95.03.14	The singular vectors horizontal resolution is increased to T42, and the perturbation initial amplitude is reduced, $\alpha = \sqrt{1.5}$.

Table 2 Major modifications in the definition of the EPS initial perturbations.

	NH		Europe	
	day 2	day 5 to 7	day 2	day 5 to 7
94.05.01 - 94.07.31	1.43	1.56	1.30	1.50
94.08.01 - 94.10.31	1.10	1.22	0.96	1.22
94.11.01 - 95.01.31	1.06	1.27	0.97	1.19
95.02.01 - 95.05.03	1.06	1.23	0.96	1.16
95.05.01 - 95.07.31	1.31	1.38	1.29	1.32
95.08.01 - 95.10.31	1.28	1.28	1.11	1.16

Table 3 Ratio among the (seasonal average) rms error of the control and the (seasonal average) rms spread, for NH and Europe, at forecast day 2 and averaged among day 5 and 7.

	Northern Hemisphere		Europe	
	day 7	day 10	day 7	day 10
94.05.01 - 94.07.31	0.03 (0.08)	0.05 (0.02)	0.02 (0.11)	0.05 (0.02)
94.08.01 - 94.10.31	0.05 (0.09)	0.10 (0.10)	0.04 (0.17)	0.11 (0.03)
94.11.01 - 95.01.31	0.04 (0.06)	0.10 (0.04)	0.05 (0.16)	0.14 (0.05)
95.02.01 - 95.05.03	0.04 (0.05)	0.10 (0.14)	0.05 (0.12)	0.11 (0.02)
95.05.01 - 95.07.31	0.02 (0.07)	0.06 (0.02)	0.03 (0.13)	0.04 (0.03)
95.08.01 - 95.10.31	0.03 (0.08)	0.08 (0.03)	0.01 (0.13)	0.13 (0.06)

Table 4 Difference between the seasonally averaged skill of the ensemble-mean and of the best ensemble member (in parenthesis) from the seasonally averaged skill of the control forecast, in terms of acc.

a) Northern Hemisphere day 5 acc

94.05.01 - 94.07.31	Low - High skill (cc=0.41)	
Small spread	15	31
Large spread	32	14
94.08.01 - 94.10.31	Low - High skill (cc=0.35)	
Small spread	17	28
Large spread	26	21
94.11.01 - 95.01.31	Low - High skill (cc=0.21)	
Small spread	17	24
Large spread	30	21
95.02.01 - 95.05.03	Low - High skill (cc=0.11)	
Small spread	23	26
Large spread	23	20
95.05.01 - 95.07.31	Low - High skill (cc=0.23)	
Small spread	19	26
Large spread	28	19
95.08.01 - 95.10.31	Low - High skill (cc=0.35)	
Small spread	14	27
Large spread	32	19

b) Europe day 5 acc

94.05.01 - 94.07.31	Low - High skill (cc=0.58)	
Small spread	14	32
Large spread	36	10
94.08.01 - 94.10.31	Low - High skill (cc=0.45)	
Small spread	11	30
Large spread	29	22
94.11.01 - 95.01.31	Low - High skill (cc=0.38)	
Small spread	10	28
Large spread	33	21
95.02.01 - 95.05.03	Low - High skill (cc=0.41)	
Small spread	14	26
Large spread	31	21
95.05.01 - 95.07.31	Low - High skill (cc=0.45)	
Small spread	14	27
Large spread	27	24
95.08.01 - 95.10.31	Low - High skill (cc=0.58)	
Small spread	15	28
Large spread	28	22

c) Northern Hemisphere day 7 acc

94.05.01 - 94.07.31	Low - High skill (cc=0.50)	
Small spread	17	31
Large spread	28	16
94.08.01 - 94.10.31	Low - High skill (cc=0.40)	
Small spread	12	28
Large spread	27	25
94.11.01 - 95.01.31	Low - High skill (cc=0.23)	
Small spread	22	25
Large spread	24	21
95.02.01 - 95.05.03	Low - High skill (cc=0.27)	
Small spread	17	30
Large spread	29	16
95.05.01 - 95.07.31	Low - High skill (cc=0.26)	
Small spread	18	25
Large spread	29	20
95.08.01 - 95.10.31	Low - High skill (cc=0.39)	
Small spread	17	30
Large spread	31	14

d) Europe day 7 acc

94.05.01 - 94.07.31	Low - High skill (cc=0.47)	
Small spread	15	25
Large spread	39	13
94.08.01 - 94.10.31	Low - High skill (cc=0.18)	
Small spread	15	29
Large spread	25	23
94.11.01 - 95.01.31	Low - High skill (cc=0.45)	
Small spread	16	31
Large spread	33	12
95.02.01 - 95.05.03	Low - High skill (cc=0.43)	
Small spread	15	26
Large spread	32	19
95.05.01 - 95.07.31	Low - High skill (cc=0.46)	
Small spread	19	26
Large spread	28	19
95.08.01 - 95.10.31	Low - High skill (cc=0.31)	
Small spread	20	25
Large spread	30	17

Table 5 Seasonal contingency tables for small/large spread, low/high skill (computed in terms of acc), for (a-b) NH and Europe at forecast day 5, and (c-d) NH and Europe at forecast day 7. The categories are defined by the average values. For each contingency table, the correlation coefficient *cc* between spread and skill is also reported.

	NH		Europe	
	day 5	day 7	day 5	day 7
94.05.01 - 94.07.31	30	26	36	28
94.08.01 - 94.10.31	20	16	23	16
94.11.01 - 95.01.31	17	15	13	11
95.02.01 - 95.05.03	19	16	10	16
95.05.01 - 95.07.31	32	28	48	34
95.08.01 - 95.10.31	27	23	38	25

Table 6 Seasonal average of the percentage of analysis values lying outside the EPS forecast range, over NH and Europe at forecast day 5 and 7, relative to the 500 hPa geopotential height field.

Configuration	ens. size	resolution	grid	time scheme	elapsed time	X-factor
32*T63L19	32	T63L19	full	Eulerian	3 hours	1
32*T106L19	32	T106L19	red	Semi-lag	6.7 hours	2.2
128*T63L19	128	T63L19	full	Eulerian	10.2 hours	3.4
(50*T106L31	50	T106L31	red	Semi-lag	15.2 hours	5.0)
Ope T213L31	--	T213L31	red	Semi-lag	2.5 hours	0.8

Table 7 Characteristics of the configurations under investigation for future developments of the EPS. For each configuration, the X-factor is defined as the ratio between its elapsed time and the elapsed time of the current EPS system (32*T63L19). For reference, the last row reports some values relative to the ECMWF operational high resolution model (T213L31).

Initial date	32*T63L19	32*T106L19	128*T63L19
94.12.12	43%	**15%**	20%
95.01.12	38%	49%	**20%**

Table 8 Percentage cf analysis values lying outside the EPS forecast range, relative to the 500 hPa geopotential height field over Europe at forecast day 7 (minimum values are highlighted).